# Supplementary Information

## Structural basis for safe and efficient energy conversion in a respiratory supercomplex

Wei-Chun Kao*, Claire Ortmann de Percin Northumberland, Tat Cheung Cheng, Julio Ortiz, Alexandre Durand, Ottilie von Loeffelholz, Oliver Schilling, Martin L. Biniossek, Bruno P. Klaholz, Carola Hunte*

*Correspondence to: wei-chun.kao@biochemie.uni-freiburg.de (W.-C.K.), carola.hunte@biochemie.uni-freiburg.de (C.H.)

**This PDF file includes:**

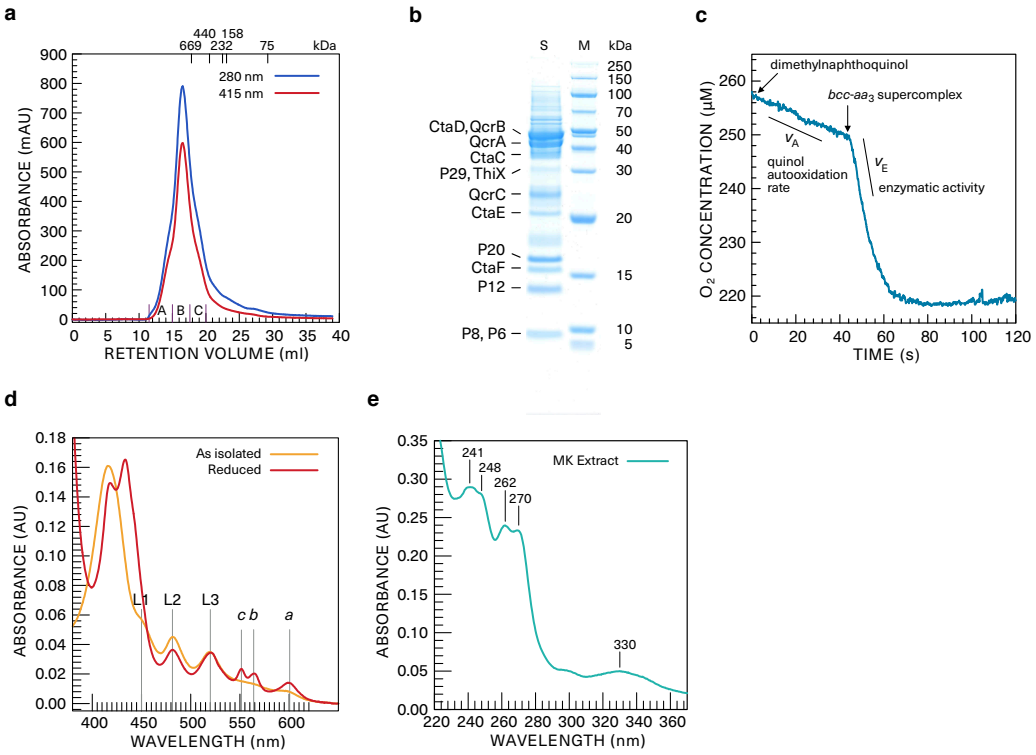


**Supplementary Fig. 1 Biochemical characterisation of the cyt *bcc-aa*$_3$ supercomplex from *Corynebacterium glutamicum***. **a** Chromatogram of final purification step by size-exclusion chromatography. The first two fractions were used for cryo-EM single particle analysis. **b** SDS-PAGE analysis of the supercomplex prior to grid preparation (Coomassie-stained gel, supercomplex lane S, molecular weight standard proteins lane M). The experiment was repeated four times and one representative gel image is shown. **c** Enzyme activity of isolated supercomplex. The dimethylnaphthoquinol:dioxygen reductase activity of 112.6 ± 3.4 $e^{-}s^{-1}$ was determined monitoring oxygen consumption. **d** UV-Vis spectroscopic analysis of the as-isolated supercomplex as well as the supercomplex reduced by 0.5 mM sodium dithionite. The three absorption maxima L1 (450 nm), L2 (481 nm), L3 (520 nm) denote the absorbance contributions from lycopene[1]. *a*, *b*, *c*, are the maximum absorbance of *a*-, *b*-, and *c*-type haems at 600 nm, 563 nm and 551 nm, respectively[2]. **e** UV-Vis spectrum of menaquinone (MK) in acidified ethanol extracted from the isolated supercomplex (for details see methods). Supercomplex concentration was determined spectroscopically[2]. The ratio of menaquinone to supercomplex monomer was determined to be 4.2:1.

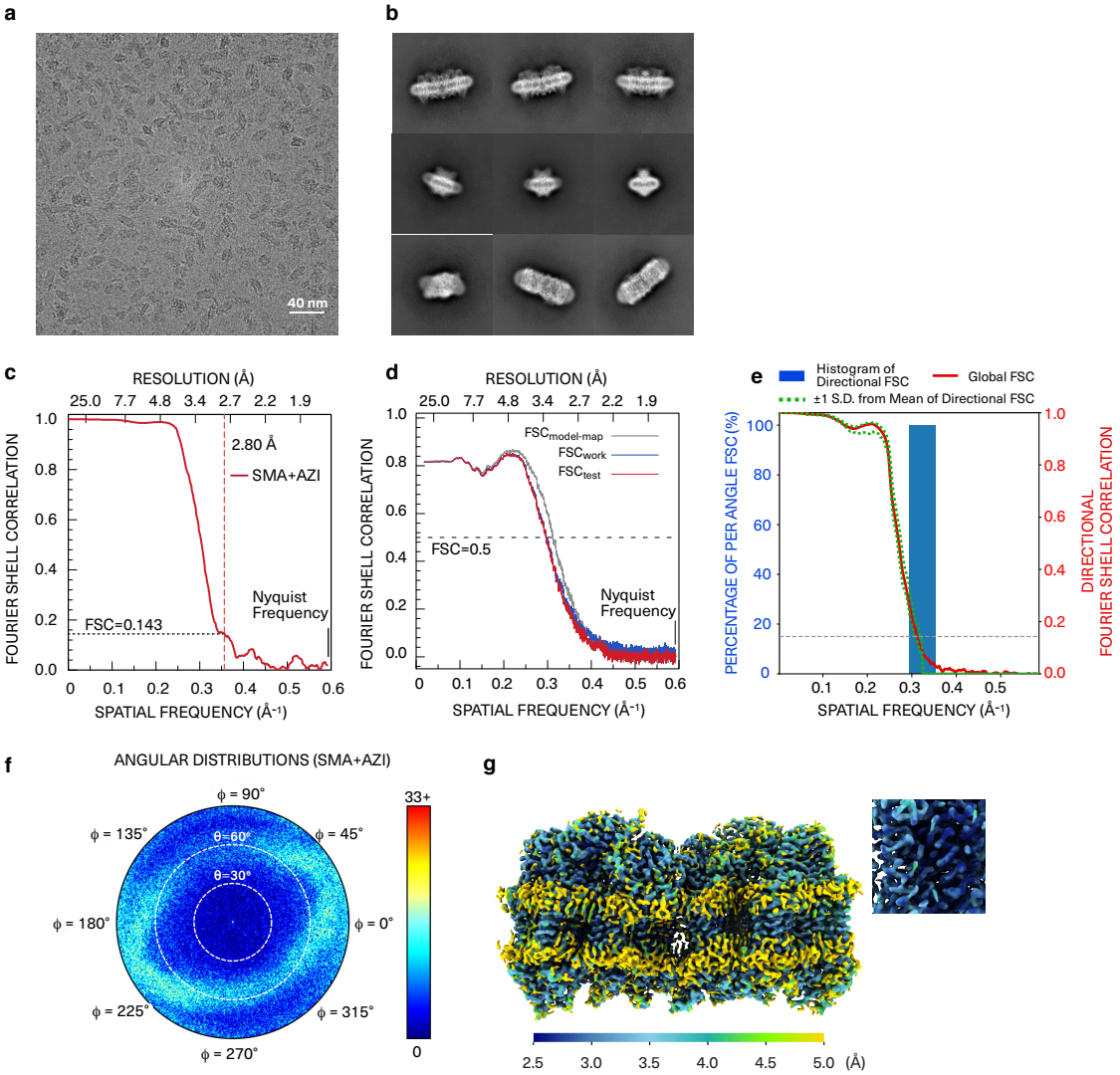


**Supplementary Fig. 2 Single particle cryo-EM analysis and validation of the stigmatellin (SMA) and azide (AZI)-treated cyt *bcc-aa*$_3$ supercomplex. a** A representative micrograph showing the diverse orientations and homogeneity of the supercomplex particles. A total number of 2833 images was collected from the same grid in one cryo-EM session and 2697 micrographs were used for structure determination (selection criteria see Methods). **b** Selected 2D-class averages of the supercomplex. **c** Fourier shell correlation (FSC) of the final 3D-reconstruction reported by cisTEM 1.0.0. **d** Cross correlation analysis **e** 3D-FSC analysis. **f** Angular distributions of supercomplex. **g** Local resolution estimated by ResMap 1.1.4. In order to visualize the supercomplex only, the detergent micelle was removed for the figure using a mask. The inset shows a selected inner part of the complex at high contour level (7 rmsd).

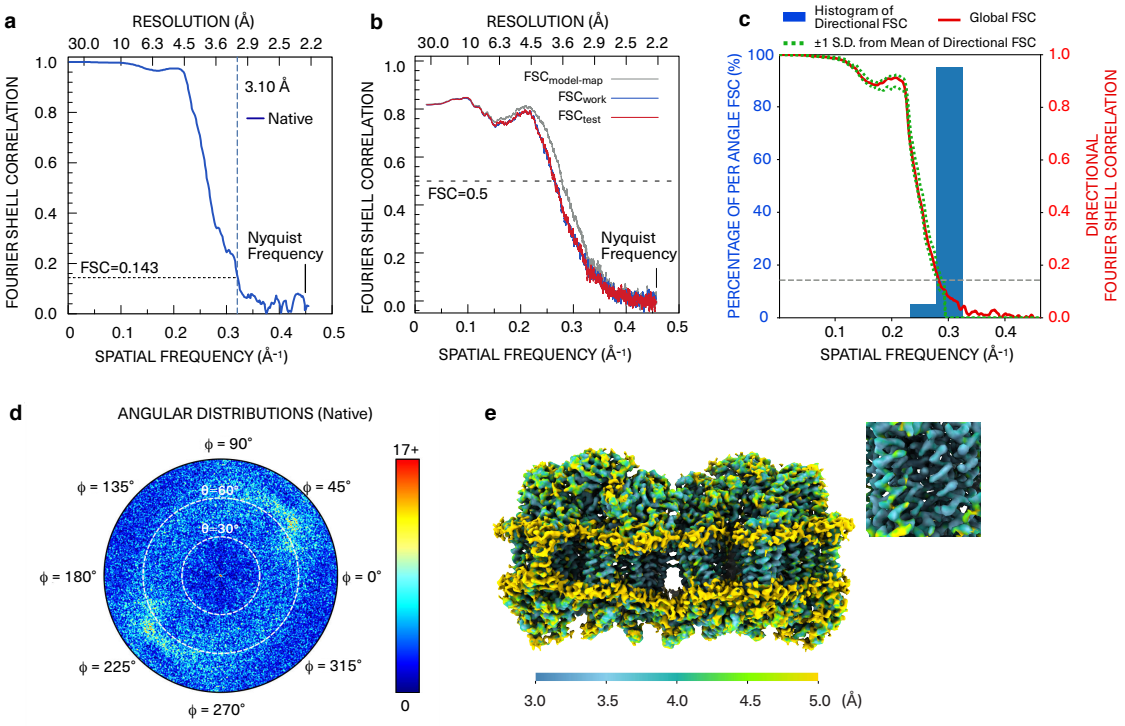


**Supplementary Fig. 3 Single particle cryo-EM analysis and validation of the as-isolated cyt *bcc-aa*$_3$ supercomplex. a** Fourier shell correlation (FSC) of the final 3D-reconstruction reported by cisTEM 1.0.0. **b** Cross correlation analysis. **c** 3D-FSC analysis. **d** Angular distributions of supercomplex. **e** Local resolution estimated by ResMap 1.1.4. In order to visualize the supercomplex only, the detergent micelle was removed for the figure using a mask. The inset shows a selected inner part of the complex at high contour level (7 rmsd).

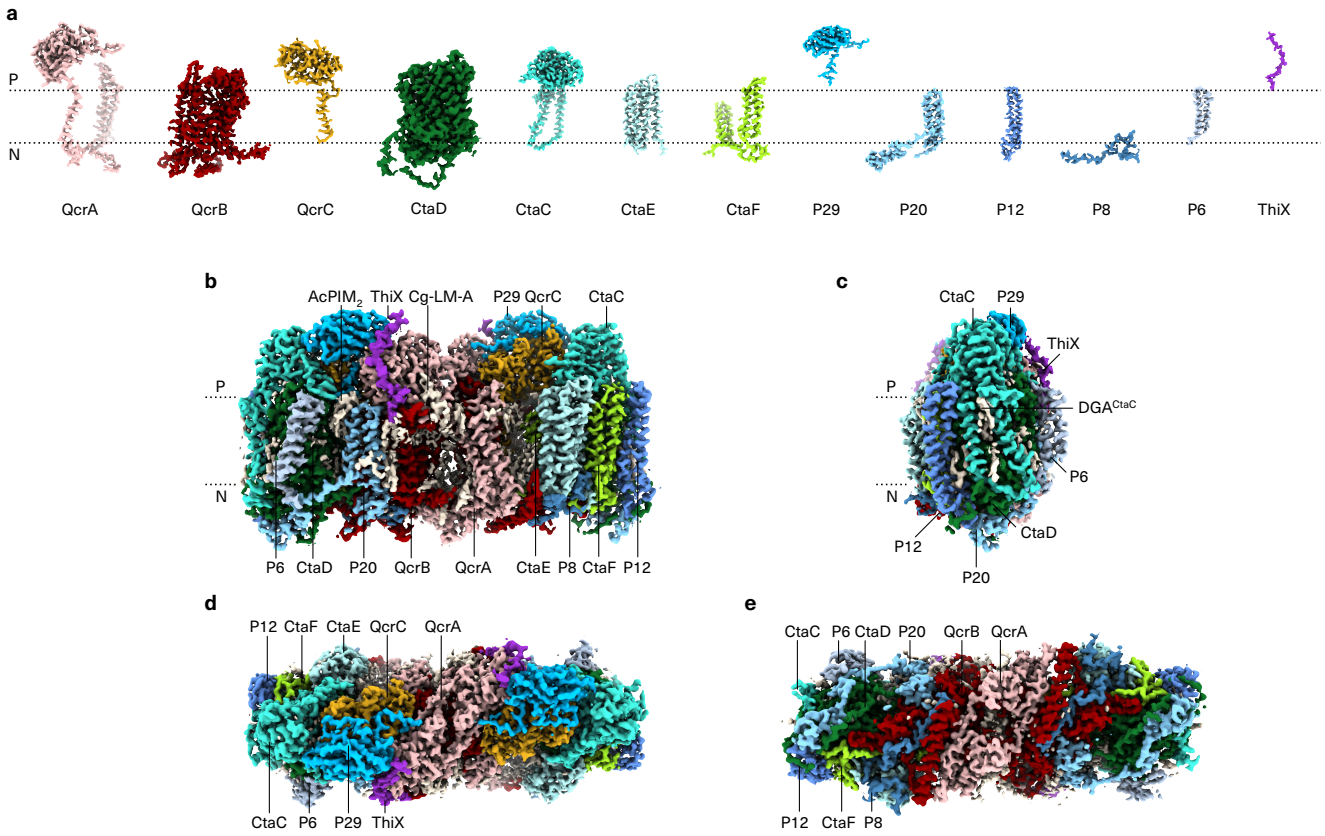


**Supplementary Fig. 4 Cryo-EM maps of subunits of *C. glutamicum* cyt *bcc-aa*$_3$ supercomplex. a** Cryo-EM map of individual subunits. The approximate membrane boundary (dotted lines) depicts the relative position of the subunits. P and N indicate the electro-positive and -negative sides of the cell membrane. **b-c** The entire complex viewed parallel to the membrane. **d** and **e** show the supercomplex from the P- and N-side of the cell membrane, respectively. The Cryo-EM map is coloured to depict the individual subunits and lipid molecules are shown in beige. Selected lipid molecules ($AcPIM_2$ and Cg-LM-A, the N-terminal covalently linked DGA of CtaC) are highlighted with labels. The contour level of the maps was set to 1.7 rmsd.

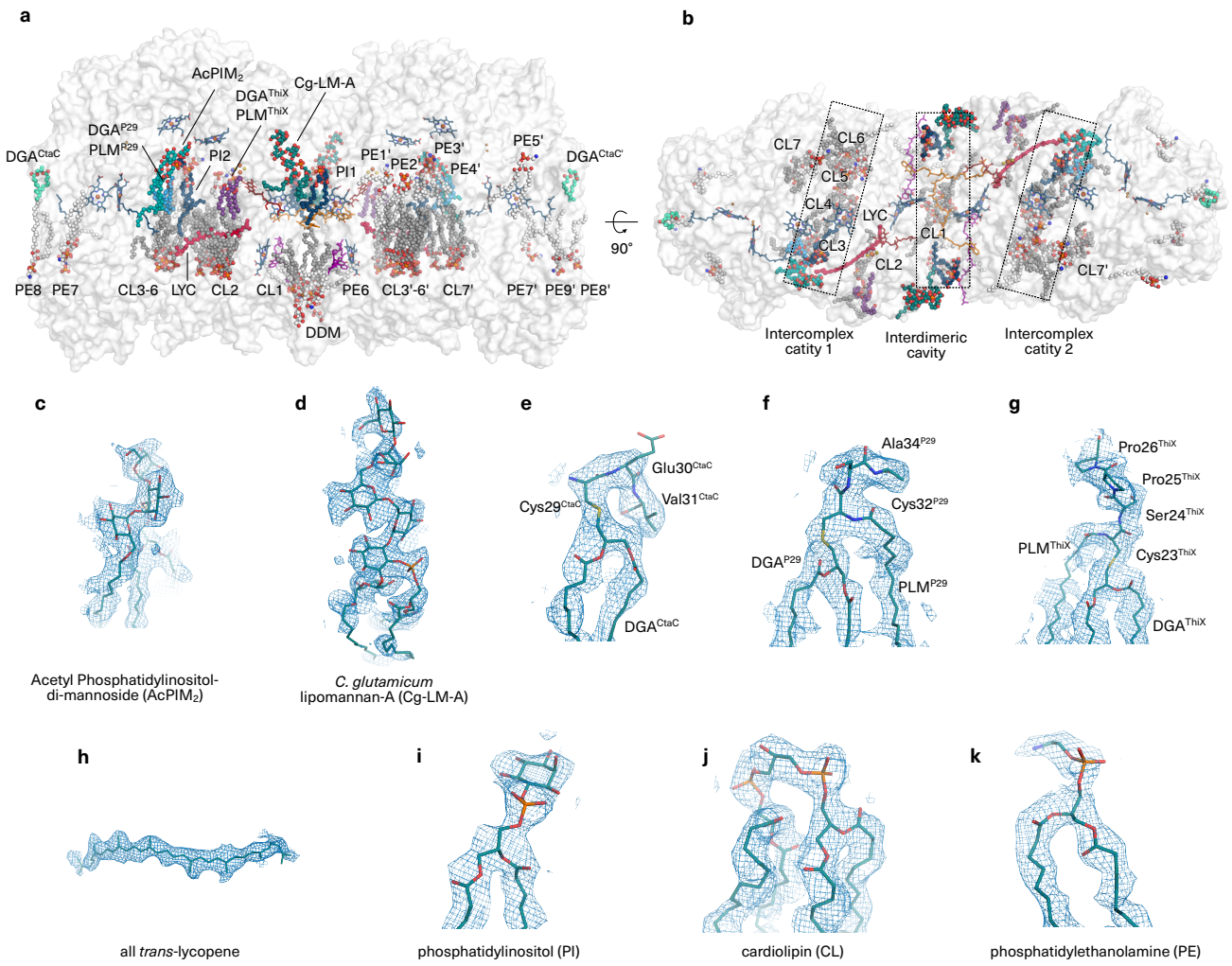


**Supplementary Fig. 5 Structural lipids, lipid-modifications and lycopene in cyt *bcc-aa*$_3$ supercomplex structure.** **a-b** Lipid molecules are shown in sphere presentation, the supercomplex in transparent surface mode with cofactors and substrates in stick presentation. PE: phosphatidylethanolamine; PI: phosphatidylinositol; CL: cardiolipin; DGA: diacylglycerol; PLM: palmitic acid; LYC: lycopene; AcPIM$_2$: acetylated phosphatidylinositol dimannoside; Cg LM-A: *C. glutamicum* lipomanman-A; DDM: dodecyl β-D-maltoside (detergent). All ligands of the dimeric complex structure are displayed. The numbering of molecules in equivalent position of both protomers are identical, but labeled with a prime (‘) for the second protomer. DGA and PLM are N-terminal modifications of the subunits indicated. **c-d** Structures and cryo-EM map (blue mesh) of glycophospholipids. **e-g** Structures and cryo-EM map (blue mesh) of the N-terminal modifications of CtaC, P29 and ThiX. **h** lycopene **i-k** examples for PI, CL and PE molecules. The contour level of all maps was set to 1.2 rmsd in all panels except to 2.0 rmsd in **g**.

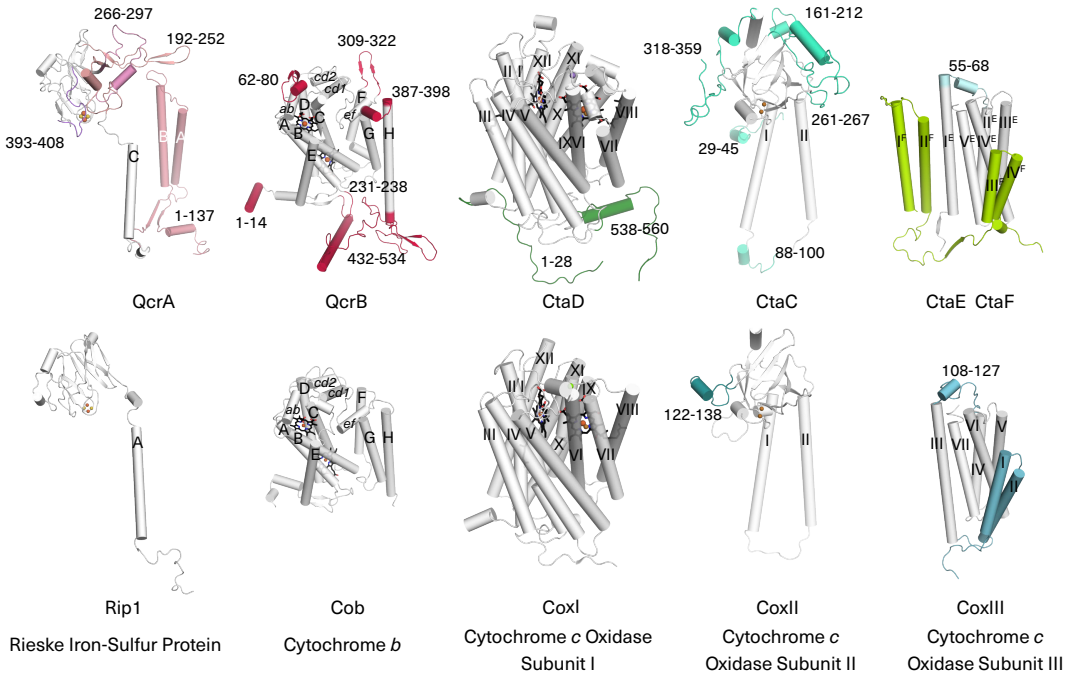


**Supplementary Fig. 6 Comparison of cyt *bcc-aa*$_3$ supercomplex subunits with homologous subunits of mitochondrial cyt *bc*$_1$ complex and cyt *aa*$_3$ oxidase.** Subunits of the supercomplex (upper row) and their mitochondrial counterparts (lower row) are presented in the same orientation in cartoon representation. Conserved structural elements are shown in white; unique parts are highlighted with their residue numbers. Nomenclature of secondary structural elements of the supercomplex follow the conventions of the yeast cyt *bc*$_1$ complex (pdb 3cx5) and bovine cyt *aa*$_3$ oxidase (pdb 5b1a). Note that CtaE is homologous to TMH III-VII of subunit COXIII. THM III-IV of CtaF are homologous to TMH I-II of COXIII.

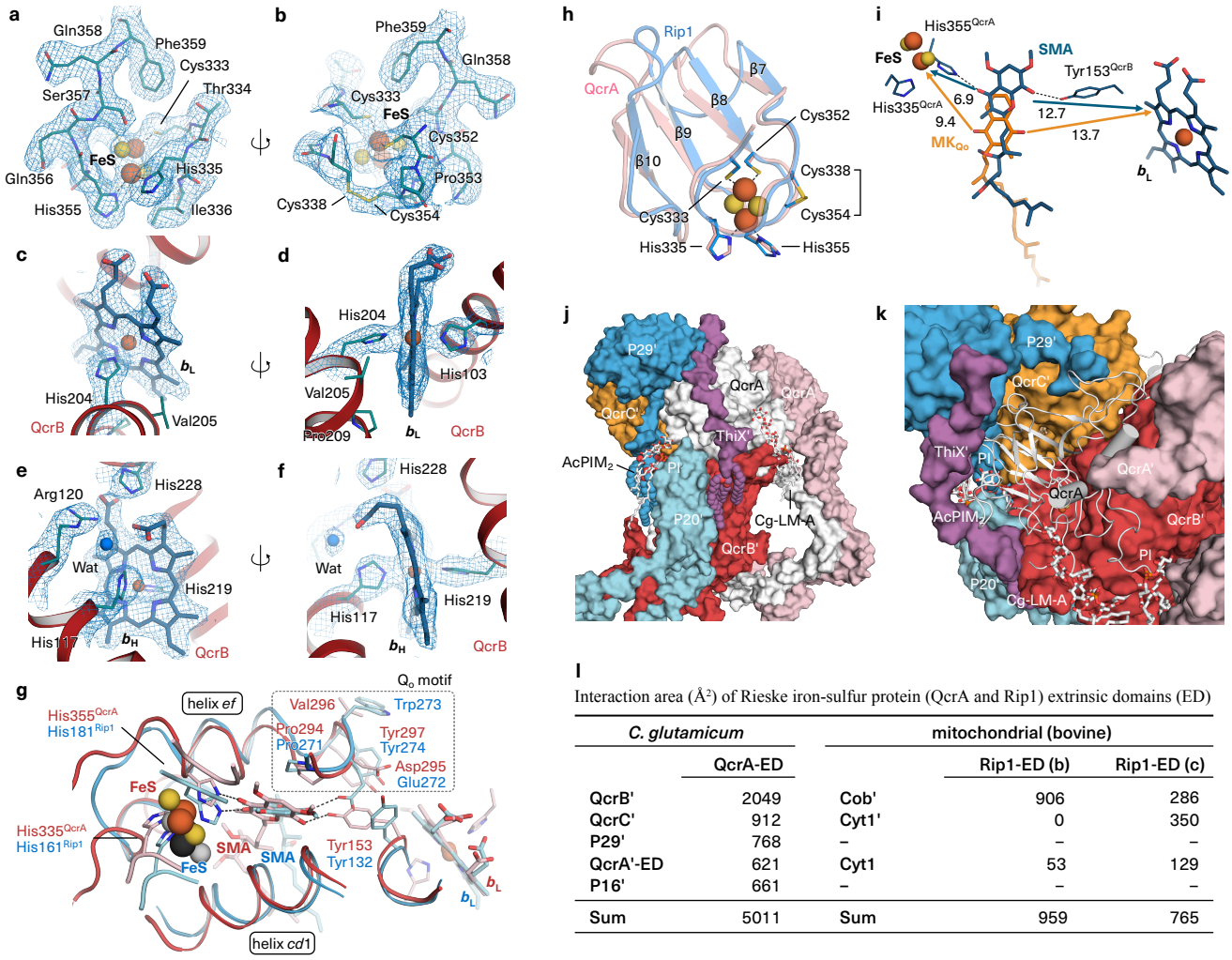


**l**

Interaction area (Å²) of Rieske iron-sulfur protein (QcrA and Rip1) extrinsic domains (ED)

| *C. glutamicum* | | mitochondrial (bovine) | | |
|---|---|---|---|---|
| | QcrA-ED | | Rip1-ED (b) | Rip1-ED (c) |
| QcrB' | 2049 | Cob' | 906 | 286 |
| QcrC' | 912 | Cyt1' | 0 | 350 |
| P29' | 768 | – | – | – |
| QcrA'-ED | 621 | Cyt1 | 53 | 129 |
| P16' | 661 | – | – | – |
| Sum | 5011 | Sum | 959 | 765 |

**Supplementary Fig. 7 Redox-cofactors of cyt *bcc* complex and interactions of subunit QcrA. a-b** Section of QcrA with Rieske iron-sulfur cluster (FeS). Residues shown belong to QcrA . **c-d** Low potential haem $b_L$ embedded in QcrB. Its axial ligand His204 is located on a π-bulge, in which Val205 is in non-bonded contact distance to haem $b_L$. Residues shown belong to QcrB. **e-f** High potential haem $b_H$ embedded in QcrB. A water molecule (Wat) coordinated by the propionate group and Arg120 is a conserved feature also found in mitochondrial cyt $bc_1$ complexes. Residues shown belong to QcrB. **g** Comparison of $Q_o$ site with bound stigmatellin (SMA) with that of mitochondrial yeast mitochondrial cyt $bc_1$ complex. The cyt *b* subunit (blue) was superposed onto the QcrB subunit (brown). $Q_o$ motifs of both complexes are highlighted in the box. The edge-to-edge distances of stigmatellin to FeS and haem $b_L$ are 6.9 and 12.7 Å, respectively, in cyt *bcc* complex, and equivalent distances in the yeast enzyme are 6.8 and 11.4 Å. Dotted lines indicated H-bonds. **h** Comparison of the FeS cluster-binding fold (QcrA, pink) with that in yeast mitochondrial cyt $bc_1$ complex (Rip1,blue, pdb 3cx5). Residues are numbered according to QcrA. Cys338 and Cys354 form a disulfide bond. **i** Comparison of stigmatellin (SMA) and menaquinone ($MK_{Qo}$) positions resolved in the $Q_o$ site. Structures of native and stigmatellin-bound supercomplex were superimposed and cofactors and ligand of the latter structure are shown in blue. This includes $Tyr153^{QcrB}$ and $His355^{QcrA}$ with H-bonds (dotted lines) to SMA. $MK_{Qo}$ is shown in orange. Respective edge-to-edge distances are given in Å. **j-k** Integration of QcrA into the complex. The N-terminal lipid modification of P29 and ThiX are shown in spheres. Subunits are shown in surface presentation, those of the other protomer are denoted with a prime (‘). Lipids ($AcPIM_2$, PI, Cg-LM-A) are shown in stick presentation. **k** QcrA in cartoon presentation to visualize its interaction to QcrB and QcrC. **l** Interface area (Å²) of the extrinsic domain (ED) of QcrA within the supercomplex and for bovine Rip1 within the cyt $bc_1$ complex. The mitochondrial Rip1-ED was resolved in different positions in X-ray structures. The “b” position close to cyt *b* (pdb 2a06) and the “c” position close to cyt $c_1$ (pdb 1be3) were used for calculation. The contour level of maps (blue mesh) was set to 2.2 rmsd in **a** and **b**; to 2.7 rmsd in **c-f**. Iron and sulfur atoms of cofactors are shown in brown and yellow spheres, respectively, water molecules as blue spheres.

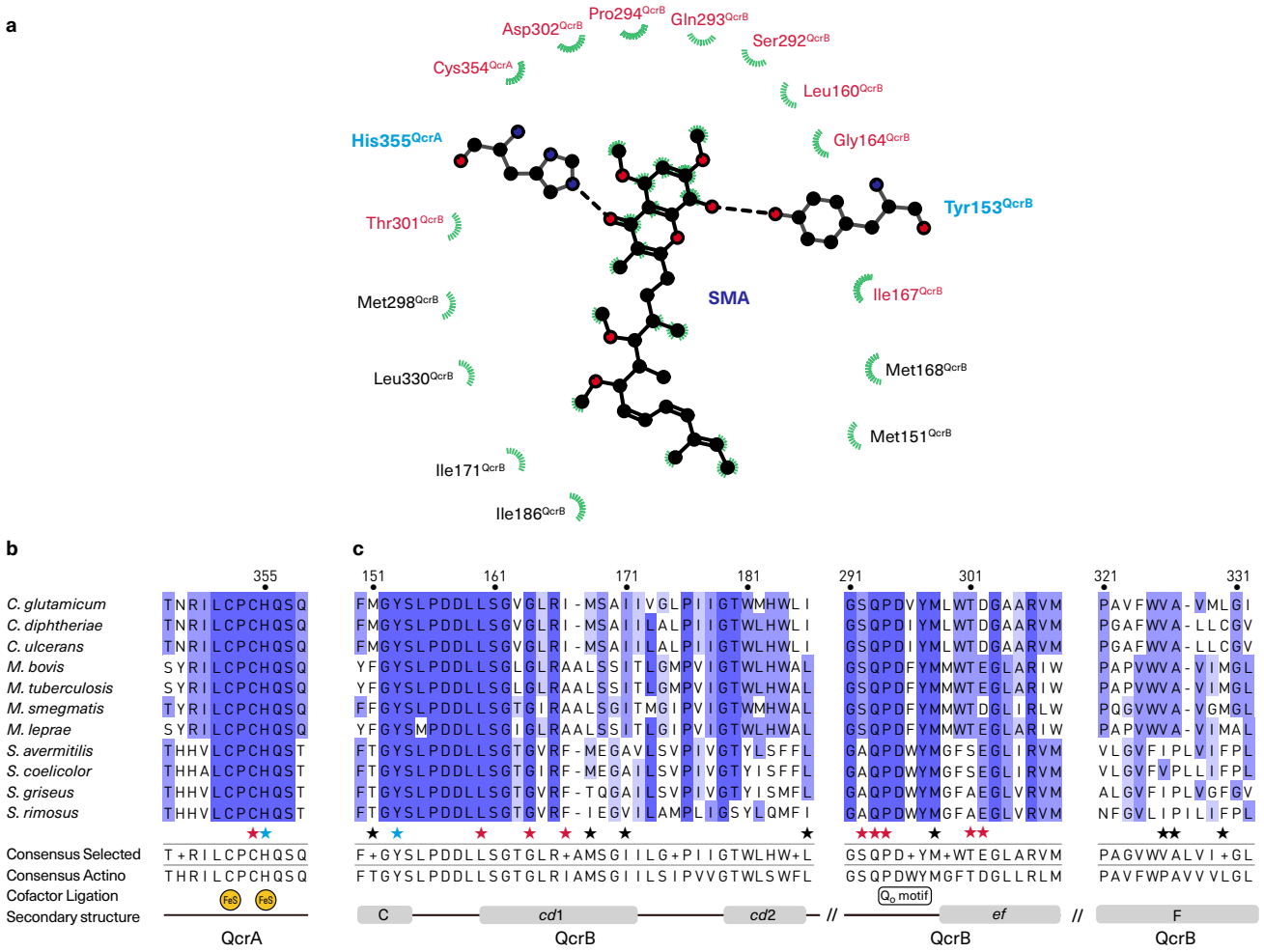


**Supplementary Fig. 8 Binding of stigmatellin in the $Q_o$ site and conservation of $Q_o$ site residues.**
**a** Residues are shown that provide direct hydrogen bonds (dotted lines) and non-bonded interactions (green dashed lines) up to 4-Å distance (blue: hydrogen bonding partners of SMA; magenta: residues which interact with the chromone ring derivative, others in black). **b, c** Multiple sequence alignment of QcrA (**b**) and QcrB (**c**) from *C. glutamicum* comparing with selected pathogenic and antibiotics-producing actinobacterial species. The full-length amino acid sequences of QcrA and QcrB were aligned using ClustalOmega (1.2.3) and sections forming the $Q_o$ site are shown. At the bottom, grey boxes indicate transmembrane and surface helices labelled in capitals and italics, respectively. The residues of the $Q_o$ motif [2] are indicated. Amino acid residues which interact with stigmatellin are indicated with a star in the same colour code as in **a**. The consensus sequence of the selected sequences as well as the consensus sequence based on all actinobacterial QcrA or QcrB with 90% identities or lower (to remove identical and highly similar sequences) are shown. NCBI Protein (https://www.ncbi.nlm.nih.gov/protein) sequence accession numbers (QcrA/QcrB): *Corynebacterium glutamicum* ATCC 13032 (NP_601394/ NP_601393), *Corynebacterium diphtheriae* NCTC 13129 (NP_939967/ NP_939966), *Corynebacterium ulcerans* 0102 (YP_006495092/ YP_006495091), *Mycobacterium bovis* AF2122/97 (NP_855867/ NP_855868), *Mycobacterium tuberculosis* H37Rv (YP_006515615/ NP_216712), *Mycobacterium smegmatis* str. MC2 155 (YP_006568914/ YP_888540), *Mycobacterium leprae* TN (NP_301666/ NP_301665), *Streptomyces avermitilis* MA-4680 (NP_827230/ NP_827231), *Streptomyces coelicolor* A3(2) (NP_626405/ NP_626404), *Streptomyces griseus* subsp. griseus NBRC 13350 (YP_001826871/ YP_001826872), *Streptomyces rimosus* subsp. rimosus ATCC 10970 (ZP_20965942/ ZP_20965943).

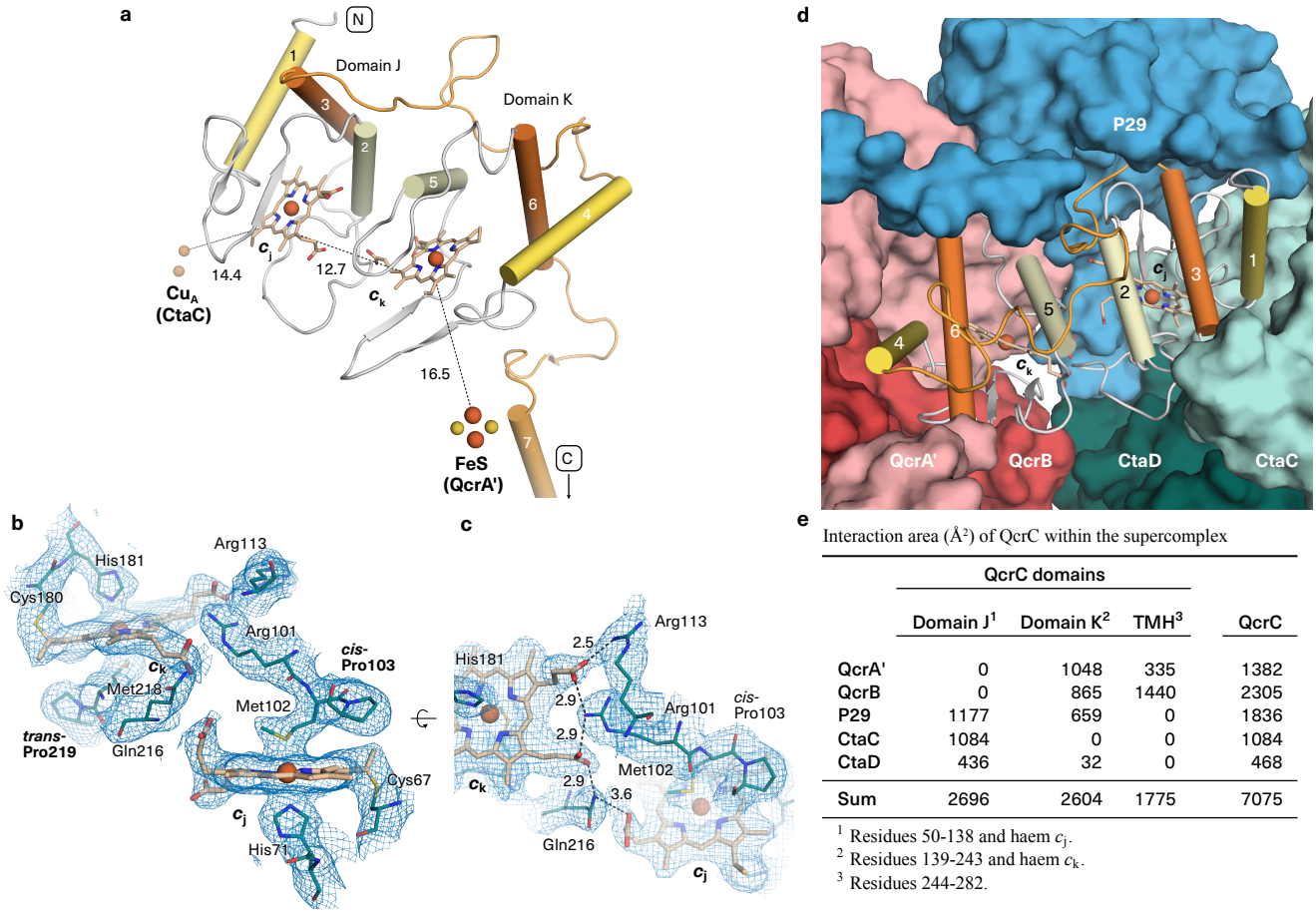


e

Interaction area (Å²) of QcrC within the supercomplex

| | QcrC domains | | | |
|---|---|---|---|---|
| | Domain J[1] | Domain K[2] | TMH[3] | QcrC |
| QcrA' | 0 | 1048 | 335 | 1382 |
| QcrB | 0 | 865 | 1440 | 2305 |
| P29 | 1177 | 659 | 0 | 1836 |
| CtaC | 1084 | 0 | 0 | 1084 |
| CtaD | 436 | 32 | 0 | 468 |
| Sum | 2696 | 2604 | 1775 | 7075 |

[1] Residues 50-138 and haem $c_j$.
[2] Residues 139-243 and haem $c_k$.
[3] Residues 244-282.

**Supplementary Fig. 9 Structure of QcrC. a** Domain composition of domain J composed of three α helices (1, 2, 3) and equivalent helices in domain K (4, 5, 6). The transmembrane helix 7 (truncated in figure) is the C-terminal transmembrane anchor. The edge-to-edge distances (dotted lines) between haem $c_j$ and haem $c_k$ and their electron transfer partners are indicated in Å. Iron atoms: brown spheres, sulfur atoms: yellow spheres. Boxed N and C denotes amino- and carboxy-termini. **b-c** Structure and cryo-EM map (blue mesh) are shown for the environment of haem $c_j$ and haem $c_k$ highlighting the interactions between the domains as well as the *cis*- and *trans*-isomers of the respective proline position in the domains. Hydrogen bonds are depicted as dashed lines and distances are in Å. All residues shown belong to QcrC. **d** Integration of QcrC in the supercomplex. QcrC shown in cartoon presentation with helices as cylinders, other subunits in surface presentation. **e** Interface area (Å²) of QcrC with adjacent subunits calculated for the entire QcrC, for its individual domains and for the transmembrane helix (TMH) using the PISA server (https://www.ebi.ac.uk/pdbe/pisa/). The boundary between J and K was defined to the middle of the connecting loop. The contour level of all maps was set to 1.8 rmsd.

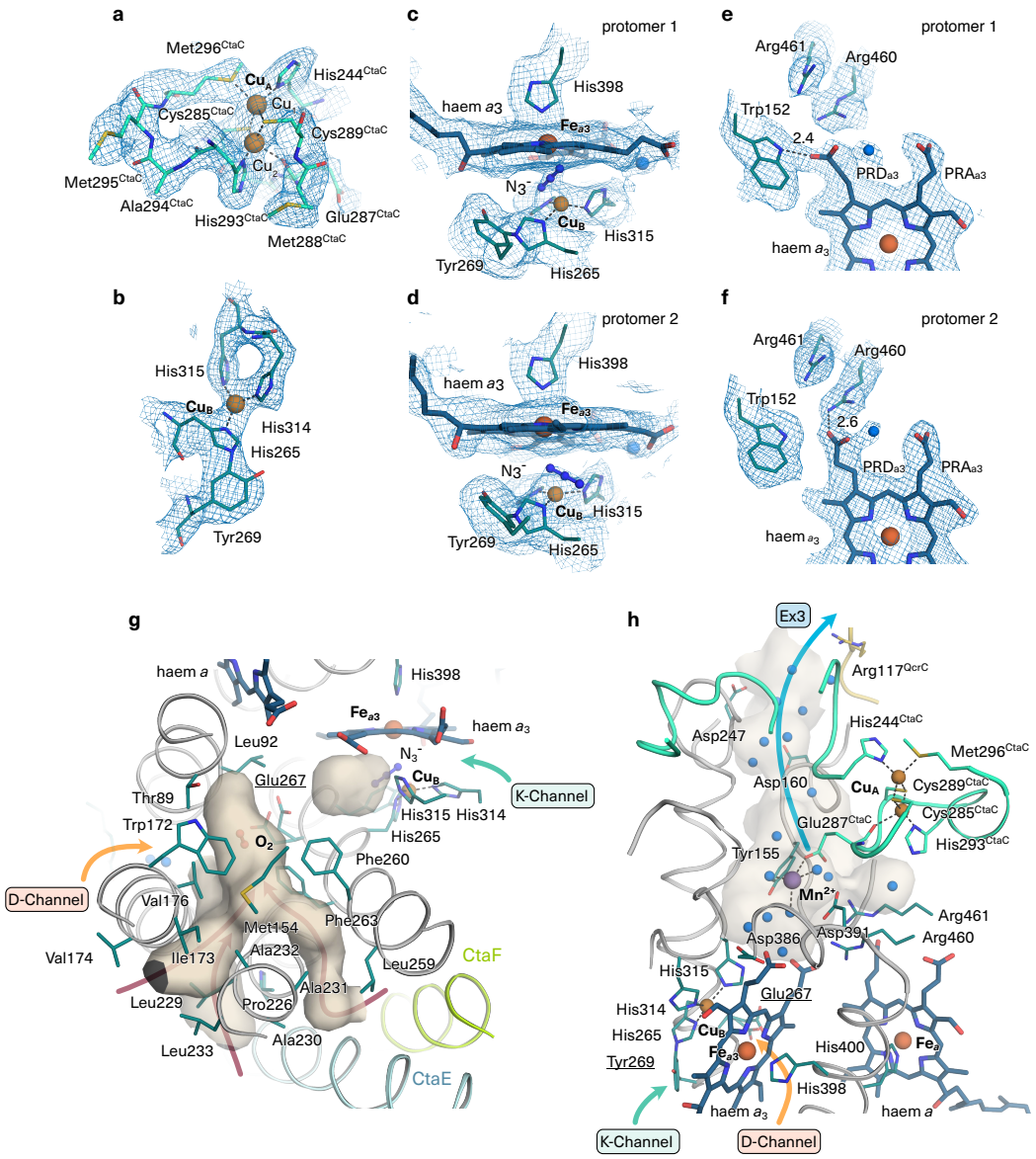


**Supplementary Fig. 10 Catalytic centres, cofactors, oxygen delivery and proton exit pathway of cyt $aa_3$ oxidase.** **a** Coordination (dotted lines) and environment of the di-copper $Cu_A$ site and **b** of $Cu_B$. All residues belong to CtaD unless noted. **c-d** Azide ions ($N_3^-$, ball-and-stick representation) resolved in protomer 1 and 2. **e-f** Close-up view of propionate δ (PRD) of haem $a_3$ in protomer 1 and protomer 2 with hydrogen-bond (dotted line), distances given in Å. **g** Oxygen tunnel (beige) with dioxygen molecule ($O_2$, ball-and-stick representation) bound, calculated with Glu267 (underlined) in up-conformation as compared to continuous tunnel in down-conformation shown in Fig. 3. The conformation constricts the tunnel above the end of the D- channel leaving a separate small cavity at the catalytic site between $Fe_{a3}$ and $Cu_B$ (marked by an azide ion ($N_3^-$) in the structure). Residues belong to CtaD (main chain in grey) unless noted CtaD. **h** Proton exit pathway (Ex3) of the oxidase. The colour code is as in **g**. Residues belong to CtaD unless noted. Tyr269 and Gl267 (both underlined) mark the end of K- and D-channel. Water molecules are shown as blue spheres. The grey Ex3 surface was computed using HOLLOW 1.3 with the radius of a water molecule. The contour level of cryo-EM maps (blue mesh) was set to 2.2 rmsd in **a**, 2.0 rmsd in **b**, 1.0 rmsd in **c-d**, 1.8 rmsd in **e**, 1.2 rmsd in **f**.

**Supplementary Table 1 | Cryo electron microscopy data collection, structure determination, refinement and validation statistics**

| | EMDB-13976<br>pdb 7QHM | EMDB-13977<br>pdb 7QHO |
|---|---|---|
| **Sample Preparation** | | |
| Protein | *Corynebacterium glutamicum* cytochrome *bcc-aa*$_3$ supercomplex | |
| Additive 1 | Stigmatellin | – |
| Additive 2 | Sodium Azide | – |
| **Data collection** | | |
| Microscope | FEI Titan Krios with Cs corrector | FEI Titan Krios with Cs corrector |
| Magnification | 75,000 | 105,000 |
| Voltage (kV) | 300 | 300 |
| Electron exposure (e$^-$Å$^{-2}$) | 40.0 | 59.7 |
| Detector | FEI Falcon3 | Gatan K2 Summit with GIF energy filter |
| Physical pixel size (Å) | 0.853 | 1.08[1] |
| Defocus range ($\mu$m) | -1.0 to -3.0 | -1.3 to -3.0 |
| Initial number of particles | 431154 | 73863 |
| Final number of particles for 3D reconstruction | 200424 | 51060 |
| Symmetry imposed | C1 | C2 |
| Box size (pixels) | 580 $\times$ 580 | 512 $\times$ 512 |
| Average map resolution (Å) | 2.80 | 3.10 |
| FSC threshold | 0.143 | 0.143 |
| **Refinement** | | |
| Initial model used | *ab initio* | *ab initio* |
| Model Resolution (Å) | 3.0 | 3.3 |
| FSC threshold | 0.5 | 0.5 |
| Chains | 26 | 26 |
| Atoms | 97686 (hydrogens: 48161) | 95896 (hydrogens: 47400) |
| Protein residues | 5886 | 5870 |
| Water molecules | 416 | 10 |
| Ligands | 88 | 78 |
| Model-to-map fit, CC_mask: | 0.80 | 0.76 |
| Bonds (r.m.s.d.) | | |
| Length (Å) (# > 4$\sigma$) | 0.009 (41) | 0.007 (30) |
| Angles (°) (# > 4$\sigma$) | 1.082 (56) | 0.960 (36) |
| *B*-factors (Å$^2$) | | |
| min/max/mean | | |
| Protein | 12.19/73.41/31.99 | 33.57/81.59/49.70 |
| Ligand | 14.31/67.44/30.74 | 33.97/70.51/48.62 |
| Water molecules | 9.43/38.85/23.46 | 39.88/48.14/44.00 |
| **Validation** | | |
| MolProbity | | |
| MolProbity score | 1.24 | 1.41 |
| Clash score | 1.87 | 4.16 |
| Ramachandran Plot (%): | | |
| Outliers | 0.14 | 0.03 |
| Allowed | 4.08 | 3.30 |
| Favoured | 95.78 | 96.67 |
| Rotamer outliers (%) | 0.71 | 0.46 |
| C$\beta$ outliers (%) | 0.00 | 0.00 |
| Peptide plane: | | |
| cis-proline: | 4.6 | 4.6 |
| cis-general: | 0.2 | 0.1 |
| twisted proline: | 0.0 | 0.0 |
| twisted general: | 0.0 | 0.0 |

[1] Movies were recorded using the super-resolution mode of 0.54 Å/pixel.

**Supplementary Table 2 | Subunit composition of the cryo electron microscopy structure of the *C. glutamicum* *bcc-aa*$_3$ supercomplex.**

| *Corynebacterium glutamicum bcc-aa*$_3$ Supercomplex | | | | | | | | | |
|---|---|---|---|---|---|---|---|---|---|
| Sub-unit | Chain ID | NCBI (UniProt) accession number | Gene name | Range resolved | Matured range | MW[1] kDa | TMH | Cofactors | Functional name |
| QcrA | A / N | NP_601394 (Q79VE8) | Cgl2190 | 5–408 | 1–408 | 45.2 | 3 | FeS | Rieske ISP |
| QcrB | B / O | NP_601393 (Q79VE9) | Cgl2189 | 1–534 | 1–539 | 59.8 | 8 | heme $b_H$ , $b_L$ | Cytochrome *b* |
| QcrC | C / P | NP_601395 (Q8NNK5) | Cgl2191 | 50-281 | 49–283[2] | 23.7 | 1 | $c_j$, $c_k$ | Di-heme cytochrome *c* |
| CtaD | D / Q | NP_601724 (Q9AEL9) | Cgl2523 | 2–560 | 1–584 | 65.1 | 12 | $Cu_B$, *a*, $a_3$ | Cyt *c* oxidase subunit I |
| CtaC | E / R | NP_601399 (Q8NNK2) | Cgl2195 | 29-359 | 29–359[3] | 36.8 | 2 | $Cu_A$, Mn | Cyt *c* oxidase subunit II |
| CtaE | F / S | NP_601396 (Q9AEL8) | Cgl2192 | 16-205 | 1–205 | 22.4 | 5 | | Cyt *c* oxidase subunit III |
| CtaF | G / T | NP_601398 (Q8NNK3) | Cgl2194 | 1-143 | 1–143 | 15.5 | 4 | | Cyt *c* oxidase subunit IV |
| P29 | H / U | NP_601863 (Q8NMB4) | Cgl2664 | 32-186 | 32–194[3] | 17.0 | 0 | | |
| P20 | I / V | NP_601222 (Q8NP09) | Cgl2017 | 9-136 | 1–147 | 16.4 | 2 | | |
| P12 | J / W | NP_599621 (Q8NTD4) | Cgl0373 | 4-112 | 1–112 | 12.1 | 2 | | |
| P8 | K / X | NP_600047 (Q8NS61) | Cgl0818 | 16-73 | 1–73 | 8.4 | 0 | | |
| P6 | L / Y | NP_599905 (Q8NSJ8) | Cgl0673 | 3-65 | 1–65 | 6.6 | 2 | | |
| ThiX | M/ Z | NP_601532 (P42461) | Cgl2332 | 23-46 | 23–190 | 17.2 | 0 | | |
| Sum | | | | | | 345.4 | 41 | | |

[1] Molecular weight of the polypeptide is calculated after post-translational processing.
[2] Predicted using the SignalP-5.0 Server with a signal peptide.
[3] Predicted using the SignalP-5.0 Server with a lipoprotein signal peptide.

**Supplementary Table 3 | Subunit composition of the cryo electron microscopy structures of the *bcc-aa*$_3$ supercomplex from *Corynebacterium glutamicum* and the homologous supercomplex from *Mycobacterium smegmatis***

| *C. glutamicum* | | *M. smegmatis* (pdb 6adq) | | | *M. smegmatis* (pdb 6hwh) | | | Identities \| Similarities (%)[1] |
|---|---|---|---|---|---|---|---|---|
| **Subunit** | **Chain** | **Subunit** | **Chain** | **rmsd[3]** | **Subunit** | **Chain** | **rmsd[4]** | |
| QcrA | A / N | QcrA | A / M | 1.63 | QcrA | B / A | 1.27 | 52 \| 66 |
| QcrB | B / O | QcrB | B / N | 1.26 | QcrB | Y / b | 1.01 | 64 \| 78 |
| QcrC | C / P | QcrC | C / O | 1.08 | QcrC | j,K / i,M[5] | 1.92[6] | 59 \| 72 |
| CtaD | D / Q | CtaD | F / R | 0.76 | CtaD | Q / V | 0.63 | 70 \| 84 |
| CtaC | E / R | MSMEG_4268 | E / Q | 1.18 | MSMEG_4268 | L / P | 1.05 | 50 \| 61 |
| CtaE | F / S | A0R049 | G / S | 0.80 | A0R049 | W / Z | 0.89 | 65 \| 80 |
| CtaF | G / T | MSMEG_4267 | H / T | 1.18 | MSMEG_4267 | S / X | 0.99 | 41 \| 55 |
| P29 | H / U | LpqE | K / W | 4.20 | – | – | – | 31 \| 46 |
| P20 | I / V | PRASF1 | D / P | 1.86 | Unknown PolyA | C / G | N/A[7] | 38 \| 54 |
| P12 | J / W | – | – | – | Unknown PolyA | D / H | N/A[7] | – |
| P8 | K / X | – | – | – | Unknown PolyA | F / J | N/A[7] | – |
| P6 | L / Y | CtaJ | I / U | N/A[8] | MSMEG_4693 | N / R | N/A[8] | – |
| ThiX | M / Z | SodC (Fitted) | Y / Z | N/A[8] | – | – | – | – |
| – | – | MSMEG_4692 | J / V | – | MSMEG_4692 | O / T | – | – |
| – | – | – | – | – | Unknown PolyA | E / I | – | – |

[1] Sequence identities and similarities are based on NCBI BLAST result of the *C. glutamicum* and *M. smegmatis* protein sequences. Similarities is taken from the positives score from BLAST, which indicate a conservative substitution or substitutions that are often observed in related proteins (https://www.ncbi.nlm.nih.gov/Class/FieldGuide/glossary.html).

[3] The averaged root mean squre deviation (Å) of the *C. glutamicum* model to *M. smegmatis* (pdb 6adq) model of the given chain.

[4] The averagedroot mean squre deviation (Å) of the *C. glutamicum* model to *M. smegmatis* (pdb 6hwh) model of the given chain.

[5] Chain j and i are the two soluble domains of QcrC, chain K and M are their respective transmembrane parts.

[6] Only the rmsd to the soluble domains of pdb 6hwh were calculated.

[7] The respective *C. glutamicum* and *M. smegmatis* subunits occupy roughly at equivalent position with respect to the entire supercomplex but rmsd was not calculated for polyalanine models.

[8] The respective *C. glutamicum* and *M. smegmatis* subunits occupy roughly at equivalent position with respect to the entire supercomplex but neither sequence nor structural homology was found.

**Supplementary Table 4 | Mass spectrometry peptide fingerprinting analysis of the *C. glutamicum bcc-aa*$_3$ supercomplex.**

| Subunit | Chain ID | Trypsin Uniq Pept | Trypsin Cover (%) | Gluc Uniq Pept | GluC Cover (%) | Chymo Uniq Pept | Chymo Cover (%) |
|---|---|---|---|---|---|---|---|
| QcrA | A / N | 183 | 82.6 | 84 | 56.6 | 140 | 79.9 |
| QcrB | B / O | 97 | 40.3 | 43 | 23.2 | 100 | 51.2 |
| QcrC | C / P | 67 | 60.4 | 43 | 68.5 | 36 | 63.8 |
| CtaD | D / Q | 0 | 0.0 | 18 | 15.8 | 82 | 51.0 |
| CtaC | E / R | 121 | 61.6 | 91 | 75.5 | 73 | 66.2 |
| CtaE | F / S | 12 | 25.9 | 0 | 0.0 | 21 | 53.4 |
| CtaF | G / T | 6 | 17.5 | 2 | 7.7 | 13 | 44.1 |
| P29 | H / U | 38 | 47.4 | 31 | 50.9 | 30 | 84.0 |
| P20 | I / V | 43 | 51.7 | 10 | 19.0 | 27 | 47.6 |
| P12 | J / W | 13 | 25.9 | 10 | 25.4 | 11 | 41.1 |
| P8 | K / X | 25 | 74.0 | 24 | 78.1 | 26 | 76.7 |
| P6 | L / Y | 0 | 0.0 | 3 | 24.6 | 7 | 41.5 |
| ThiX | M / Z | 3 | 11.6 | 21 | 68.1 | 19 | 44.7 |

* Uniq Pept: number of unique peptides identified; Cover = coverage, the ratio of total length of peptides identified to that of the protein sequence; GluC = endoproteinase GluC; Chymo = chymotrypsin.

**Supplementary Table 5 | Degree of sequence conservation (%) of residues in proton transfer pathways of cyt *bcc* complex in Actinobacteria.** Unless noted, all residues belong to subunit QcrB. The analysis was performed based on alignments of non-redundant sequences[2]. Values less than 0.5% are not shown.

| | Ex1 | | | | | Ex2 | | | En1 | |
|---|---|---|---|---|---|---|---|---|---|---|
| | Asp387 | Arg306 | Asp302 | His355[1] | Pro294 | Tyr153 | Asp295 | Glu260[2] | Glu38 | Lys253 |
| Asp | 99.5 | – | 55.9 | – | – | – | 100 | 3.2 | – | 1.9 |
| Glu | – | – | 44.1 | – | – | – | – | 95.8 | 99.1 | 0.5 |
| His | – | – | – | 100.0 | – | – | – | – | – | 0.9 |
| Tyr | – | – | – | – | – | 99.5 | – | – | – | – |
| Arg | – | 99.5 | – | – | – | – | – | – | – | – |
| Lys | – | – | – | – | – | – | – | – | – | 94.8 |
| Gln | – | – | – | – | – | 0.5 | – | – | – | 0.5 |
| Asn | – | – | – | – | – | – | – | – | – | 0.5 |
| Pro | – | – | – | – | 100.0 | – | – | – | – | – |
| Thr | – | – | – | – | – | – | – | – | – | – |
| Ser | – | – | – | – | – | – | – | – | – | – |

[1] QcrA
[2] QcrC

**Supplementary Table 6 | Degree of sequence conservation (%) of residues in proton transfer pathways of cyt $aa_3$ oxidase in Actinobacteria.** Unless noted, all residues belong to subunit CtaD. The analysis was performed based on alignments of non-redundant sequences[1]. Values less than 0.5% are not shown.

| | D-channel | | | | | | | | | K-Channel | | | |
|---|---|---|---|---|---|---|---|---|---|---|---|---|---|
| | Glu453[1] | His529 | Asp116 | Thr36 | Asn105 | Asn123 | Tyr45 | Thr97 | Glu267 | Glu110[2] | Ser280 | Lys341 | Thr338 |
| Asp | – | – | 98.2 | – | – | – | – | – | – | – | – | – | – |
| Glu | 97.6 | – | – | – | – | – | – | – | 98.6 | 100.0 | – | 1.1 | – |
| His | – | 91.8 | – | – | – | – | – | – | – | – | – | – | – |
| Tyr | – | – | – | – | – | – | 98.2 | – | – | – | – | – | – |
| Arg | – | 5.0 | – | – | – | – | – | – | – | – | – | – | – |
| Lys | – | – | – | – | – | – | – | – | – | – | – | 97.8 | – |
| Gln | 0.5 | – | – | – | – | – | – | – | – | – | – | 0.7 | – |
| Asn | – | 0.7 | – | – | 98.2 | 97.8 | – | – | – | – | – | – | – |
| Pro | – | – | – | – | – | – | – | – | – | – | – | – | – |
| Thr | – | – | – | 98.2 | – | – | – | 92.1 | – | – | 40.9 | – | 98.2 |
| Ser | – | – | – | – | – | – | – | – | – | – | 57.3 | – | – |

[1] QcrB
[2] CtaC

**Supplementary Table 7 | Compositions of D- and K- proton channels and the proton loading site of cyt $aa_3$ oxidases of which X-ray or cryo-EM structures are available.** The assignment of the constituent residues was referenced to the *Paracoccus denitrificans* structure[3]. Unless noted, all the amino acid residues are in CtaD or COX I (subunit I). The name-giving residues are highlighted in bold typeface. *Corynebacterium glutamicum*: this work; *Mycobacterium smegmatis*: pdb 6adq/ 6hwh; *Paracoccus denitrificans*: pdb 3hb3; *Rodobacter sphaeroides*: pdb 1m56; *Bos taurus*: pdb 5b1a; *Saccharomyces cerevisiae*: pdb 6ymy.

The D-Channel

| *C. glutamicum* | | *M. smegmatis* | | *P. denitrificans* | | *R. sphaeroides* | | *B. taurus* | | *S. cerevisiae* | | Note |
|---|---|---|---|---|---|---|---|---|---|---|---|---|
| His | 529 | His | 528 | His | 541 | His | 549 | His | 503 | His | 525 | |
| **Asp** | 116 | **Asp** | 115 | **Asp** | 124 | **Asp** | 132 | **Asp** | 91 | **Asp** | 92 | |
| Thr | 36 | Thr | 35 | Thr | 26 | Thr | 24 | Thr | 10 | Thr | 11 | |
| Asn | 123 | Asn | 122 | Asn | 131 | Asn | 139 | Asn | 98 | Asn | 99 | |
| Asn | 105 | Asn | 104 | Asn | 113 | Asn | 121 | Asn | 80 | Asn | 81 | |
| *Gly | 126 | Ser | 125 | Ser | 134 | Ser | 142 | Ser | 101 | Ala | 102 | |
| Gly | 102 | Gly | 101 | Gly | 109 | Gly | 117 | Gly | 76 | Gly | 77 | |
| Thr | 97 | Thr | 96 | Ile | 104 | Ile | 112 | Met | 71 | Met | 72 | |
| Ser | 183 | Thr | 182 | Ser | 193 | Ser | 201 | Ser | 157 | Ser | 158 | |
| Glu | 267 | Glu | 266 | Glu | 278 | Glu | 286 | Glu | 242 | Glu | 243 | |

* Gly126 can be compensated by Ser 186 to establish the equivalent hydrogen bonded network.

The K-Channel

| *C. glutamicum* | | *M. smegmatis* | | *P. denitrificans* | | *R. sphaeroides* | | *B. taurus* | | *S. cerevisiae* | | Note |
|---|---|---|---|---|---|---|---|---|---|---|---|---|
| Glu | 110 | Glu | 95 | Glu | 78 | Glu | 101 | Glu | 62 | Glu | 82 | CtaC/ SU II |
| Ser | 280 | Ser | 279 | Ser | 291 | Ser | 299 | Ser | 255 | Ser | 256 | |
| **Lys** | 341 | **Lys** | 340 | **Lys** | 354 | **Lys** | 362 | **Lys** | 319 | **Lys** | 319 | |
| Tyr | 269 | Tyr | 268 | Tyr | 280 | Tyr | 288 | Tyr | 244 | Tyr | 245 | |
| Thr | 338 | Thr | 337 | Thr | 351 | Thr | 359 | Thr | 316 | Thr | 316 | |

The Proton Loading Site

| *C. glutamicum* | | *M. smegmatis* | | *P. denitrificans* | | *R. sphaeroides* | | *B. taurus* | | *S. cerevisiae* | | Note |
|---|---|---|---|---|---|---|---|---|---|---|---|---|
| His | 315 | His | 314 | His | 326 | His | 334 | His | 291 | His | 291 | |
| Arg | 460 | Arg | 459 | Arg | 473 | Arg | 481 | Arg | 438 | Arg | 438 | |
| Arg | 461 | Arg | 460 | Arg | 474 | Arg | 482 | Arg | 439 | Arg | 439 | |
| Glu | 287 | Glu | 275 | Glu | 218 | Glu | 254 | Glu | 198 | Glu | 223 | CtaC/ SU II |
| Val | 318 | Ala | 317 | Thr | 329 | Thr | 337 | Thr | 294 | Ile | 294 | |
| Asp | 386 | Asp | 385 | Asp | 399 | Asp | 407 | Asp | 364 | Asp | 364 | |
| Asp | 256 | Asp | 244 | Asp | 193 | Asp | 229 | Asp | 173 | Asp | 198 | CtaC/ SU II |
| Lys | 254 | Lys | 242 | Lys | 191 | 227 | 362 | Lys | 171 | Lys | 196 | CtaC/ SU II |
| Phe | 387 | Phe | 386 | Arg | 400 | Arg | 408 | Leu | 365 | Val | 365 | |
| Ala | 390 | Thr | 389 | His | 403 | His | 411 | His | 368 | His | 368 | |

## Supplementary References


1. Radu, A. I. *et al*. Toward food analytics: fast estimation of lycopene and β-carotene content in tomatoes based on surface enhanced Raman spectroscopy (SERS). *Analyst* **141**, 4447–4455 (2016).

2. Kao, W.-C. *et al*. The obligate respiratory supercomplex from Actinobacteria. *Biochim. Biophys. Acta* **1857**, 1705–1714 (2016).

3. Koepke, J. *et al*. High resolution crystal structure of *Paracoccus denitrificans* cytochrome *c* oxidase: New insights into the active site and the proton transfer pathways. *Biochim. Biophys. Acta* **1787**, 635–645 (2009).